SLAC–PUB–7425
CERN LHC Project Report 95
February 1997

A Simulation Study of Electron-Cloud Instability and Beam-Induced Multipacting in the LHC*

Frank Zimmermann

Stanford Linear Accelerator Center
Stanford University, Stanford, CA 94309, USA

In the LHC beam pipe, photoemission and secondary emission give rise to a quasi-stationary electron cloud, which is established after a few bunch passages. The response of this electron cloud to a transversely displaced bunch resembles a short-range wakefield and can cause a fast instability. In addition, beam-induced multipacting of the electrons may lead to an enhanced gas desorption and an associated pressure increase. In this paper we report preliminary simulation results of the electron-cloud build-up both in a dipole magnet and in a straight section of the LHC at top energy. The effective wakefield created by the electron cloud translates into an instability rise time of about 25 ms horizontally and 130 ms vertically. This rise time is not much larger than that of the resistive-wall instability at injection energy.

(Submitted for Publication)

*Work supported by the US Department of Energy under contract DE–AC03–76SF00515.

1 Introduction

The LHC is the first hadron storage ring with a significant synchrotron radiation and an accompanying large number of photoelectrons. The total number of photons emitted per turn is comparable to that for the positron ring (LER) of the PEP-II B factory, under construction at SLAC. While in PEP-II an antechamber absorbs ∼99% of the photons, this is not the case for the LHC, and, therefore, the total number of photons hitting the beam screen per meter is about 5 times higher.

At a beam energy of 7 TeV, the critical photon energy in a dipole magnet is 44 eV. For this photon energy, the photoemission yield (i.e., the number of photoelectrons per incident photon) is about 0.1. The emitted photoelectrons are accelerated by the beam field to an energy of a few 100 eV. Since, for most materials, the secondary emission yield for incident electron energies above 100 eV is larger than 1, these photoelectrons generate more secondary electrons, when they again hit the beam screen.

Therefore, an avalanche production of secondary electrons becomes possible, where the electron density increases with every new bunch passing by. Our simulation indicates that the build-up of the electron cloud saturates when the repelling electron space charge on average neutralizes the field of the beam. The stationary electron cloud can be removed by a gap in the bunch train, after which the electron-cloud build-up commences again.

beam energy E (GeV)	7000
number of particles / bunch N_b	1.05×10^{11}
beam current I (A)	0.54
h. r.m.s. beam size σ_x (mm)	0.303
v. r.m.s. beam size σ_y (mm)	0.303
r.m.s. bunch length σ_z (cm)	7.7
bunch spacing L_{sep} (m)	7.48
bend length l_b (m)	14.2
bend field B (T)	8.4
bending radius ρ (m)	2780
circumference C (km)	26.66
vacuum screen half height h (mm)	18.5
vacuum screen half width w (mm)	23
horizontal tune Q_x	63.28
vertical tune Q_y	63.31

Table 1: LHC parameters assumed for this study; from Ref. [3].

Transverse multi-bunch instabilities attributed to photoelectrons interacting with a train of positron bunches have recently been reported from the KEK photon factory [4, 1] and from BEPC at IHEP in Bejing [5]. An instability of this kind, with a millisecond rise time, is also predicted for the LER of the PEP-II B factory [6, 7, 8]. The electron-cloud instability, sometimes called the 'Ohmi effect' [1], was experimentally found to occur for short bunch spacings [4], where the photoelectrons cross the beam pipe within a few bunch passages.

Conversely, it has been known since the mid-70s from beam tests with an Al chamber prototype in the ISR [2] that, in the opposite regime of larger bunch spacings, beam-induced multipacting is possible. Here, electrons bounce from wall to wall in resonance with the discrete bunch structure, and, if the secondary emission yield is larger than

unity, the number of electrons amplifies exponentially. Increased gas desorption and a local pressure bump were the observable harmful effect [2]. The LHC parameters, listed in Table 1, allow for multipacting, with an approximate threshold of 160 mA total beam current [9]. Although they occur for different values of the bunch spacing, electron-cloud instability and multipacting are both caused by the same physical processes and no clear distinction is possible. The LHC parameters lie on the border line where either effect can be important.

It may be worthwhile to mention that in the ISR also an electron-driven instability of a coasting proton beam has been observed [10, 11]. The most important differences between the LHC and the ISR are: 1) the LHC beam is bunched and 2) the enormous number of primary photoelectrons in the LHC.

2 Physics Model and Some Numbers

The number of photons emitted by a charged particle per radian is [12]

$$N_\gamma = \frac{5}{2\sqrt{3}}\ \alpha\ \gamma \tag{1}$$

where α is the fine-structure constant and γ the Lorentz factor. In the LHC at 7 TeV, this amounts to about 3.7×10^{10} photons per 14.2-m long bend and per proton bunch. For comparison, assuming 1 nTorr hydrogen gas at 10 K, about 3×10^4 electrons per bend and per bunch are generated by ionization of the residual gas. This number is more than 6 orders of magnitude smaller than the number of photoelectrons, which illustrates the significance of the synchrotron radiation in the LHC!

A typical photoemission yield at energies of 10–100 eV is 0.1, see, e.g., Ref. [13]. According to Ref. [14], the reflectivity of the beam pipe material for these photon wavelengths is close to 90%. Thus, one might assume [15] that on average a photon is either reflected or converts into a photoelectron, so that the final total number of photoelectrons is approximately equal to the number of radiated photons, or that the 'effective photoemission probability' η_{pe}^{eff} is equal to 1. This is the assumption made in our simulation. Under this assumption, every photon is reflected up to 10 times before it creates a photoelectron, and the impact location on the beam screen can be considered random. For this reason, we launch the photoelectrons uniformly distributed around the beam-screen aperture (idealized as elliptic), with an initial uniform energy distribution between 0 and 10 eV.

It has been conjectured by M. Zisman [16] that the reflectivity of a real beam pipe can be much lower, perhaps as low as 5–10%, in which case we would overestimate the emitted photoelectrons by almost an order of magnitude. We have, therefore, evaluated the sensitivity of the final electron density to the photoemission yield. In general, after an initial transient, the build-up and maintenance of the electron cloud is largely determined by the secondary emission, whereas the dependence on the photoemission parameters is not too critical (a similar result was obtained in simulations of the electron-cloud instability for PEP-II [15]).

Photoelectrons emitted from the wall are accelerated by the field of the beam. A photoelectron generated by synchrotron radiation of the bunch head acquires the maximum transverse momentum:

$$\Delta p_{el} \approx \frac{2 N_b r_e c m_{el}}{r_{pipe}} \tag{2}$$

where r_e denotes the classical electron radius, c the speed of light, r_{pipe} the radius of the beam pipe, m_{el} the electron mass and p_{el} the electron momentum. For the LHC parameters, $\Delta p_{el}/m_{el} \approx 0.028\ c$, corresponding to an energy of

$$\Delta E_{el} \approx \frac{1}{2} m_{el} c^2 \ \left(\frac{v}{c}\right)^2 \approx 200 \text{ eV} \tag{3}$$

and to a wall-to-wall time of flight of about 1.5 m/c. Photoelectrons created by radiation from later parts of the bunch only receive a fraction of the 200-eV maximum energy, and their wall-to-wall time of flight is accordingly larger. Since the bunch spacing is 7.5 m, most of the primary photoelectrons hit the wall, before the next bunch arrives. When an electron of energy ∼200 eV impinges on the wall, secondary electrons are emitted. The velocity of these secondary electrons is a factor 5–10 lower than that of the incident electron. These secondary electrons are accelerated, along with the newly generated photoelectrons, when the next bunch passes by. Thus, without an electron space-charge force, the number of electrons would increase indefinitely.

Most of the LHC circumference is occupied by high-field dipole magnets in which the electron motion is effectively constrained to the vertical direction. The electron cloud in the dipoles is believed to be the dominant 'wakefield' source. Nevertheless, straight sections account for about 20% of the LHC circumference and the electron dynamics is different enough to motivate a separate study.

In a vertical magnetic field B of 8.4 Tesla, a 200-eV electron rotates on a circle in the x-z plane with a Larmor radius of about

$$\rho_{el} \approx \frac{p_{el}}{eB} \approx 6\ \mu\text{m} \tag{4}$$

Since during a bunch passage the horizontal kick is averaged over ∼100 cyclotron rotations, with a very small net momentum transfer [17], in dipole magnets we only apply a vertical kick from the beam. By contrast, in a straight section, the electron receives both a horizontal and a vertical kick from each passing bunch.

The potential at the beam center is given by

$$U \approx \frac{\lambda}{2\pi\epsilon_0} \ln \frac{r_{pipe}}{\sqrt{2}\sigma_y} = \frac{Z_0 I}{2\pi} \ \ln \frac{r_{pipe}}{\sqrt{2}\sigma_y} \tag{5}$$

where λ denotes the charge line density, Z_0 (=377 Ω) the vacuum impedance, and I the beam current. The average potential is about 120 V, the peak potential (due to bunching) is about 4.2 kV. This number may serve as an estimate for the maximum energy an electron close to the center of the beam pipe might receive in the bunch field.

Many aspects of secondary emission have been discussed in the literature, e.g., in Ref. [18]. In our simulation we have implemented the universal yield curve discussed by Seiler [19], where the secondary emission yield is characterized by two parameters: the primary energy at which the yield is maximum (E_p^m, assumed to be 400 eV) and the maximum yield (the emitted charge per primary charge) for perpendicular incidence, δ_{max}. We have varied δ_{max} between 1.1 (for TiN coated surfaces) and 1.8 (for OFHC copper). The analytical expression for the yield is [19, 20]

$$\delta(E_r, \theta) \approx \delta_{max}\ 1.11\ (E_r)^{-0.35}\ (1 - e^{-2.3\ E_r^{1.35}})/\cos(\theta) \tag{6}$$

with θ denoting the angle of incidence with respect to the surface normal and $E_r \equiv E_p/E_p^m$, where E_p is the energy of the incident electron. Figure 1 shows the yield δ, Eq. (6), as

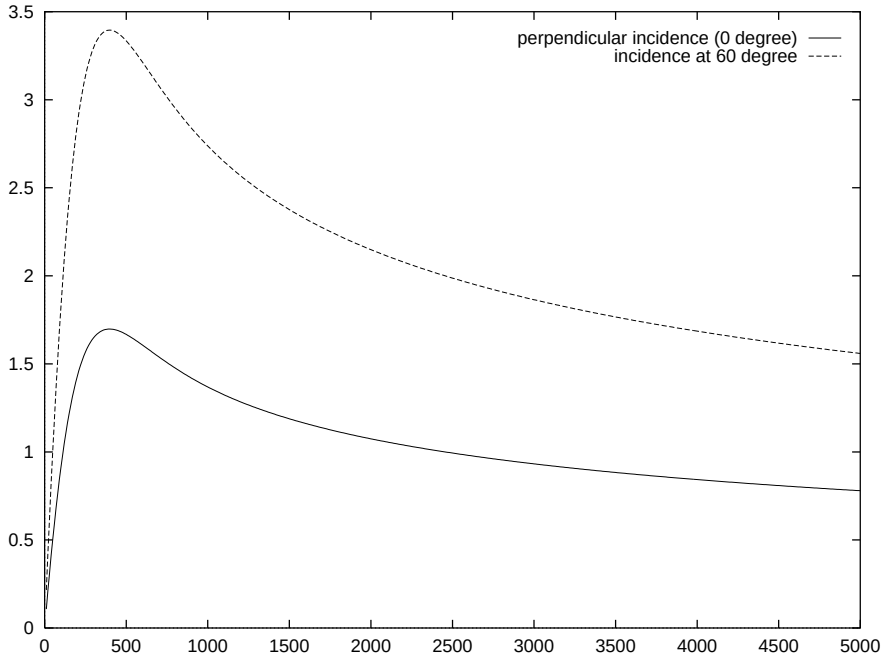

Figure 1: Secondary emission yield, Eq. (6), as a function of the primary electron energy (in eV), for 0° and 60° incident angle with respect to the surface normal, and for $\delta_{max} = 1.7$.

a function of energy, for two different values of the angle θ. To avoid unphysically large yields, we limit the $1/\cos\theta$ factor to a maximum value of 5. This cut-off is fairly arbitrary at this moment, and could be improved by measurements of the angular-dependent emission yield on beam-screen prototypes.

The energy of the emitted secondary electrons is taken to be uniformly distributed between 1 and 20 eV. Their initial velocity direction is assumed to follow a $\cos\theta$ distribution, with preferred emission in the normal direction [19]. These assumptions will have to be revised, if a 9-T magnetic field is shown to have a strong effect on the secondary emission yield and on the emission direction.

We consider each proton bunch as a uniform longitudinal charge distribution of total length $2\sqrt{2}\,\sigma_z$. The bunches are assumed to pass at the center of the beam pipe and are given a constant round cross section. Ignoring the distortion of the beam field due to the slight asymmetry between the horizontal and vertical beam-screen dimensions [21], we calculate the kick on the electrons from a passing bunch using the round-beam formula for free space

$$\Delta\vec{p}_{el} = -\frac{2N_b r_e \vec{r} m_{el}}{r^2}\left(1 - \exp\left(-\frac{r^2}{2\sigma^2}\right)\right) \tag{7}$$

where $\vec{r}$ is the position of the electron with respect to the center of the beam pipe, $r = |\vec{r}|$, and $\sigma = \sigma_x = \sigma_y$.

We represent the 4×10^{10} photoelectrons generated per bunch and per bend by a set of macroparticles of variable number. Typically we generate 1000 macro-photoelectrons for each bunch, which we distribute over the bend length of 14.2 m. The macroparticle charge of about 4×10^7 e is chosen such that the total photoelectron charge is equal to the real one.

We split each bunch into five slices. After each slice we launch new photoelectrons and apply a kick from the beam. The gap between two bunches is divided into a number

of steps (typically 7–20). At each step the motion of all macroelectrons is calculated.

When an electron hits the beam screen, we launch one or more secondary electrons at the point of impact, with charge, energy and velocity calculated as described above. The total charge of the emitted secondaries depends on the energy and on the incident angle of the lost electron. In the simulation, the number of re-emitted secondary macroelectrons is always chosen high enough that their charge is less or equal to, but never larger than that of the primary photoelectrons [22]. This prevents the undesirable situation that most of the electron charge is carried by very few macroparticles.

In order to limit the growth of the electron cloud, the electric space-charge field of the electrons is included in the simulation as well. So far, we treat this field in a rough approximation. We assume a radial symmetry and introduce a radial grid of 500 equally spaced circles. Counting the number of electron macroparticles in the different circles, we calculate the electric field at each radial grid point using Gauss' law. Between two grid points we interpolate the field linearly. As for the beam kick, in a dipole magnet the space-charge kick is applied only in the vertical direction, because of the high cyclotron frequency.

Calculating the space-charge force in the way described, we implicitly assume a radial symmetry. As we shall see, this is not always a good approximation. A more accurate simulation would use a two-dimensional FFT of the electron distribution [23] or a two- (three-) dimensional particle-in-cell simulation. We believe though that our approximate treatment is adequate to obtain a first estimate of the equilibrium density and of the instability rise time.

In the simulation, the inclusion of the space charge leads to a saturation of the electron-cloud density at a value close to the neutralization level, which we define by the number of photoelectrons that is equal to the time-averaged number of protons.

After a series of bunches have passed, we displace one bunch vertically or horizontally by a certain offset Δy or Δx, and calculate the kick that the disturbed electron cloud exerts on the following bunch. More specifically, for both dipoles and straight sections, we calculate an effective short-range dipole wake function W_1, integrated over the circumference, by summing the kicks on the bunch from all the macroelectrons:

$$W_{1,y}(L_{sep}) = \sum_i \frac{2 y_i Q_i}{N_b r_i^2 \ (\Delta y)} \left(1 - \exp(-\frac{r_i^2}{2\sigma^2}\right) \frac{C}{l_b} \tag{8}$$

where L_{sep} denotes the bunch spacing, C the ring circumference, l_b the length of a bending magnet, Q_i the charge of the ith macroelectron, y_i (x_i) its vertical (horizontal) coordinate and r_i the radial distance from the center ($r_i \equiv \sqrt{x_i^2 + y_i^2}$). An equivalent expression holds for the horizontal plane. Due to the peculiar nature of the electron cloud, this wake-function definition could depend on the magnitude of the offset Δy (or Δx) chosen.

To obtain the integrated wake function of the LHC, we take a weighted average over the two different regions considered, i.e.,

$$W^{LHC}_{1,y\ (x)}(L_{sep}) \approx 0.8 \times W^{bend}_{1,y\ (x)} + 0.2 \times W^{straight}_{1,y\ (x)} \tag{9}$$

where the factors 0.8 and 0.2 are the relative fractions of the LHC circumference that are covered by bending magnets and straight sections, respectively.

From the effective wake functions $W_{1,y}$ and $W_{1,y}$ the instability rise times can be computed. To obtain a first rough estimate, we consider a train of $M = 3564$ proton bunches (equal to the maximum number of bunch places) uniformly distributed around

the ring. Assuming that the wakefield decays rapidly and only affects the next bunch, the complex multibunch betatron frequency shift is [1, 24]:

$$\Omega^{(\mu)} - \omega_\beta = \frac{N_b r_p c^2}{2\gamma C \omega_\beta}\, W_1(L_{sep})\; e^{i2\pi(\mu + Q_{y\ (x)})/\mu} \qquad \text{for} \qquad \mu = 0, ..., M-1 \tag{10}$$

where $Q_{y\ (x)}$ is the vertical (horizontal) betatron tune. The imaginary part of Ω^μ is the instability growth rate of the μth multibunch mode. The instability spectrum is very broadband and covers many modes. The shortest rise times of the fastest growing modes are of the order

$$\tau \approx \frac{2\gamma C \omega_\beta}{N_b r_p c^2 W_1(L_{sep})} \tag{11}$$

If there are clearing gaps and the ring is not uniformly filled, the amplitude of the nth consecutive bunch increases as

$$y_n \sim \frac{1}{n!} \left(\frac{N_b r_p c^2 t}{2\gamma C \omega_\beta}\right)^n \hat{y}_0 \tag{12}$$

where t is the time and $\hat{y}_0$ an initial perturbation of the first bunch in the train. For large values of n, Eq. (12) approaches an exponential behavior with a time constant identical to that in Eq. (11).

3 Simulation Results

Figure 2 presents a typical electron-charge build-up inside a bending magnet. The charge increase as a function of time is shown for two different secondary-emission yields. As can be seen, in both cases the charge density saturates after the passage of less than 10 bunches. The neutralization density for these parameters corresponds to a total electron charge of about 2×10^{11} e, which is not far from the saturation values observed in Fig. 2. Figure 3 (top) compares the unlimited charge increase without space charge with the saturated behavior that is observed when the electron space charge is included. The repelling space-charge field is calculated using the approximation outlined above. An example is shown in Fig. 4. The space-charge field increases roughly linearly with the radius, which would be consistent with a fairly uniform electron distribution.

Almost all the results discussed in this report were obtained assuming a photon reflectivity of 90%. If the real reflectivity is lower, less photoelectrons will be emitted. Figure 3 (bottom) shows how, in the simulation, the electron cloud builds up more slowly, when the number of photoelectrons is reduced.

In Fig. 5, the transverse macroparticle distribution established after 40 bunches is depicted for two different secondary-emission yields δ_{max}. For large values of δ_{max} (bottom figure), two broad vertical stripes of increased electron density emerge. The path of a macroelectron and of all its descendants is constrained to the same horizontal position by the magnetic field, which leads to the appearance of many narrow vertical lines compounding these two stripes. The two vertical stripes are located at a horizontal distance of about $\pm 20\sigma$ (6 mm) from the beam-pipe center. Figure 6 shows that at this horizontal position the maximum electron energy after the passage of a bunch is about equal to the characteristic energy E_p^m for which the secondary-emission yield is maximum (see Fig. 1). Figure 7 demonstrates that the high-density region moves towards the center, when the beam current is decreased, as one might expect.

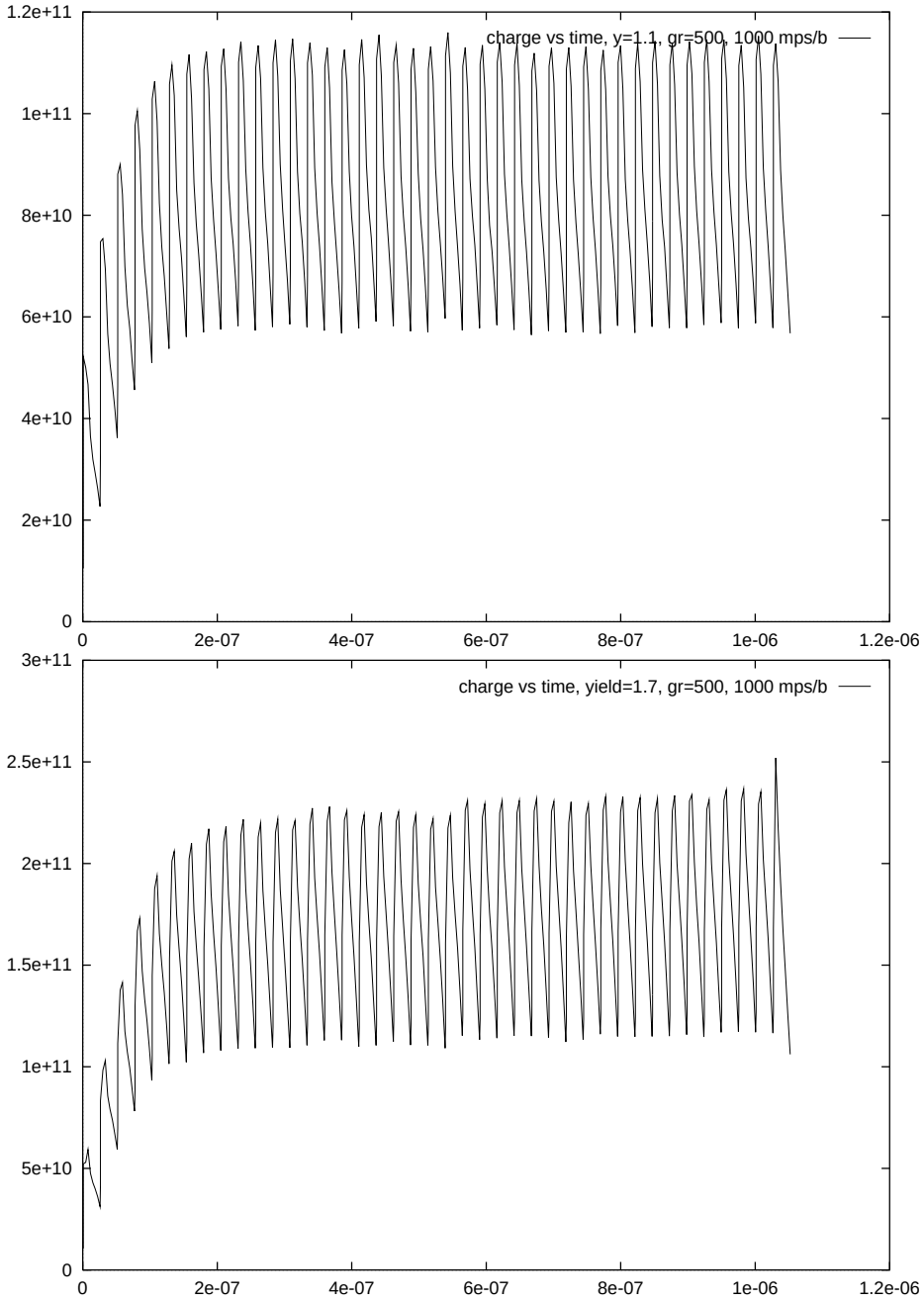

Figure 2: Charge of the electron cloud (in units of e) accumulated inside a bending magnet as a function of time (in s), for two different values of the maximum yield δ_{max}; top: $\delta_{max} = 1.1$; bottom: $\delta_{max} = 1.7$. The total time span corresponds to 41 bunch passages, which are reflected in the sawtooth-like evolution pattern. In this simulation, 1000 macroparticles per bunch were launched, and the grid size was 500 points.

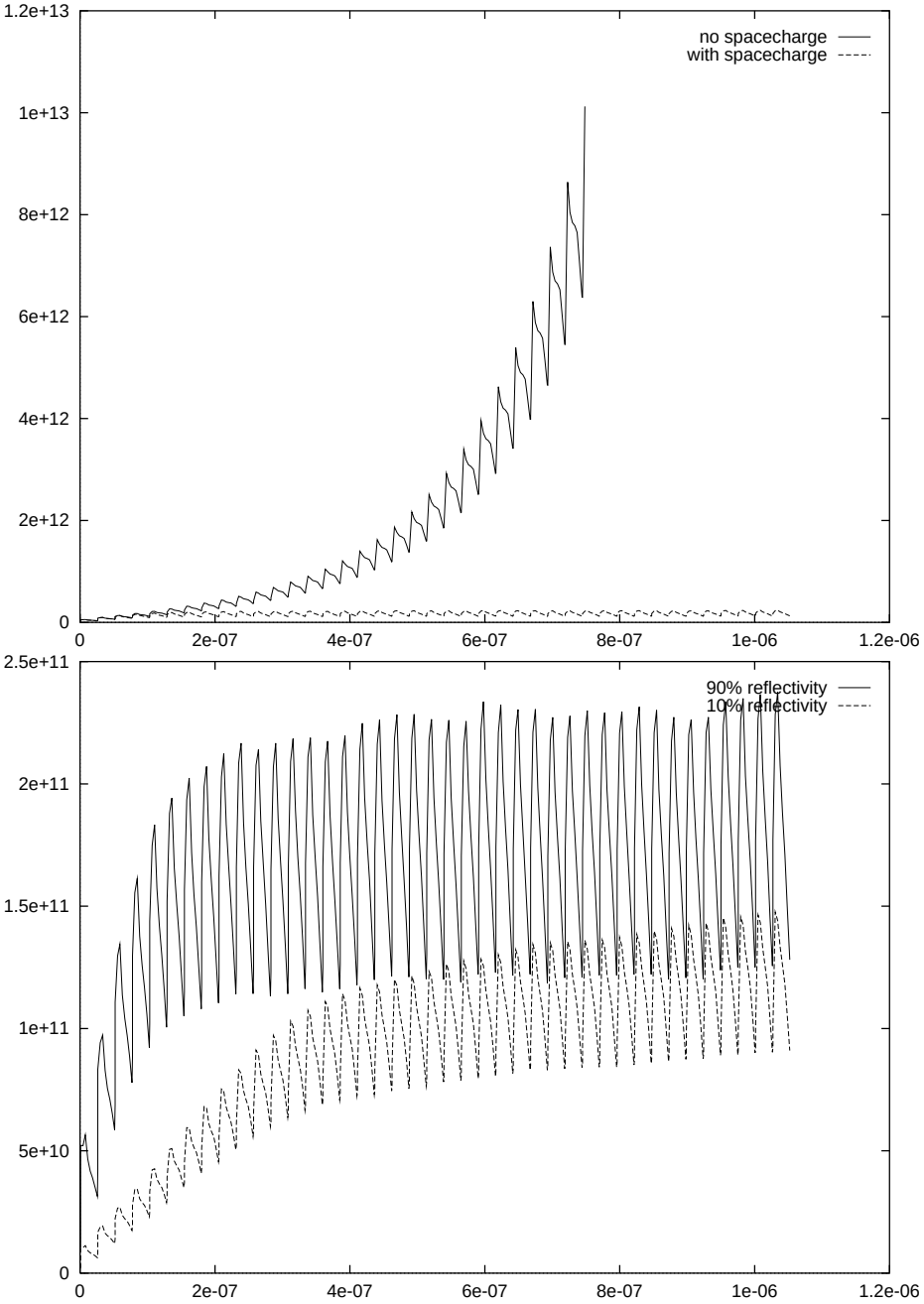

Figure 3: Charge of the electron cloud (in units of e) accumulated in a bending magnet as a function of time (in s); top: with and without space charge; bottom: with an emission probability η_{pe}^{eff} of 1 photoelectron/photon (corresponding to 90% photon reflectivity at the beam screen) and with an effective emission probability of only 0.2 photoelectrons per photon (for a reduced photon reflectivity). A maximum secondary-emission yield δ_{max} of 1.5 was assumed.

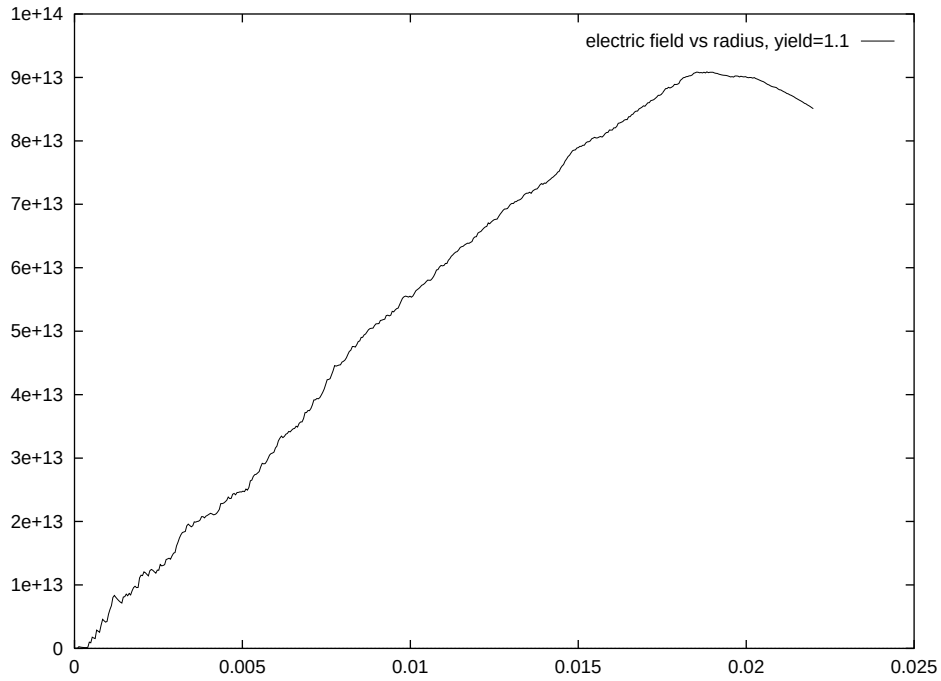

Figure 4: Electron acceleration (in m/s^2) due to the electric self-field of the electron cloud as a function of radius (in m), after 40 bunches for a maximum yield of $\delta_{max} = 1.1$.

Projected horizontal and vertical electron charge distributions are displayed in Figs. 8 and 9. Comparison of the top and bottom figures shows that the observed large fluctuations in the simulation results are of statistical nature, due to the finite number of macroparticles, and can be reduced by averaging over several random seeds. Figure 10 illustrates the perturbation of the horizontal charge distribution that is induced by a horizontally displaced bunch. It is this perturbed distribution that causes the wakefield effect.

A typical variation of the deduced wake functions for different random seeds is depicted in Fig. 11. In order to obtain reliable estimates of the dipole wake function W_1, we usually performed simulations for 10 different random seeds. For each random seed, we computed the average of the kicks for a positive and a negative offset—correcting for the relative sign of kick and offset—, to further reduce the statistical fluctuation of the result.

Simulation results for a variety of conditions are summarized in Table 2. The horizontal wakefield in the bending magnets is found to be the predominant effect. A probable reason for this is the increased and nonuniform charge density in the horizontal plane (see Figs. 8 and 10).

The computed wake functions are fairly independent of the bunch offset Δy (Δx) chosen, but the statistical error increases when the displacement is reduced. Simulations performed with varying numbers of macroparticles give almost identical results. Similarily, increasing the number of tracking steps between bunches only has a small impact on the result.

Lowering the maximum secondary-emission yield from 1.5 to 1.1 reduces the wakefield by less than a factor of 2. The moderate dependence of the wakefield on the secondary-emission yield suggests that the wakefield is not fully determined by the secondary emission, but that the photon reflectivity, the photoemission yield and the initial photoelectron

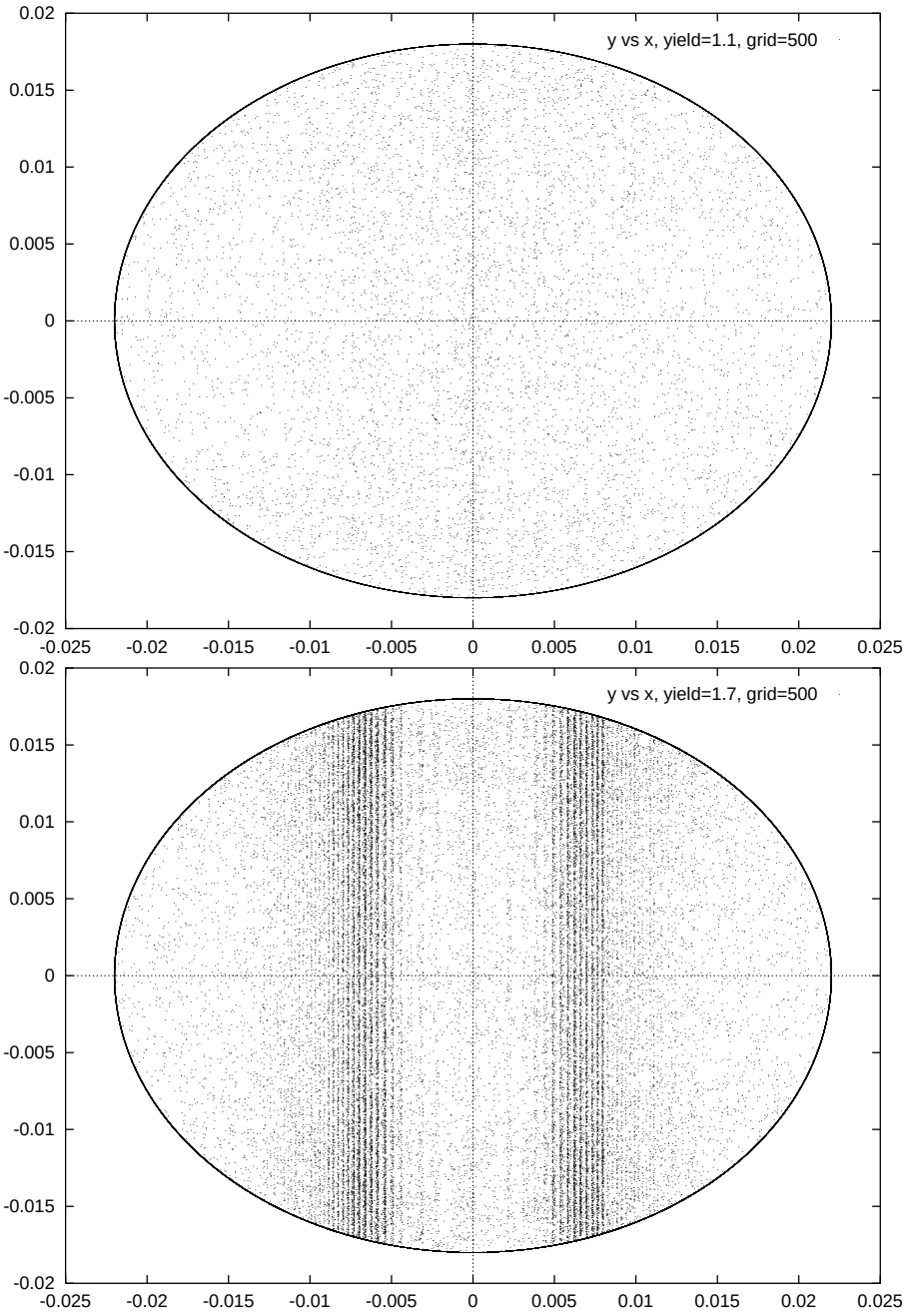

Figure 5: Transverse distribution of macroelectrons after 40 bunches for a maximum secondary emission yield δ_{max} of 1.1 (top) and 1.7 (bottom). Horizontal and vertical dimensions are given in units of m.

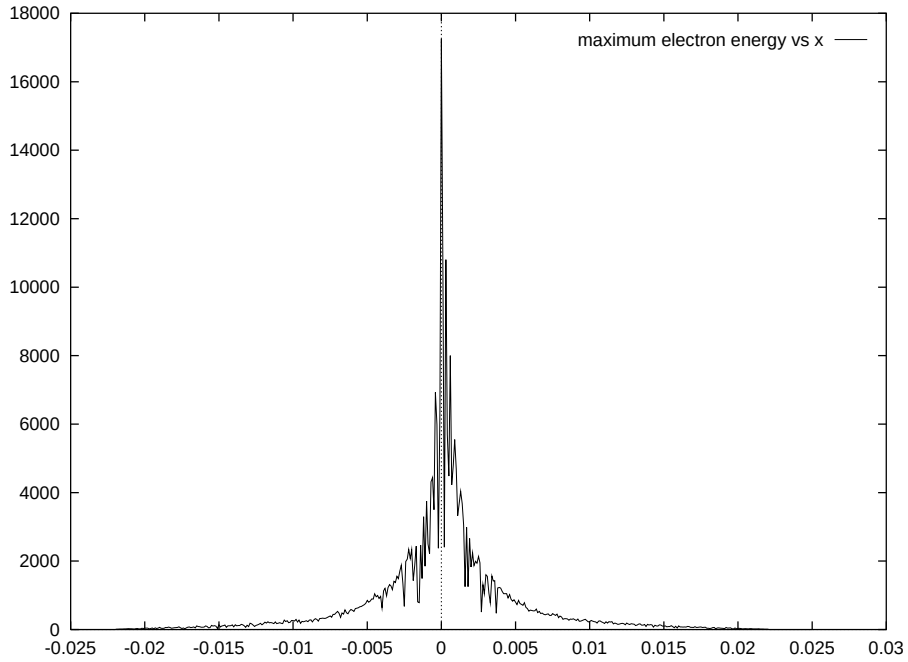

Figure 6: Maximum electron energy (in eV) after the passage of the 41st bunch as a function of the horizontal electron position (in m). Energies with maximum secondary-emission yield ($\sim$400 eV) are found about 5–8 mm from the beam-pipe center. This could explain the strong nonuniformity of the horizontal distribution seen in the bottom part of Fig. 5.

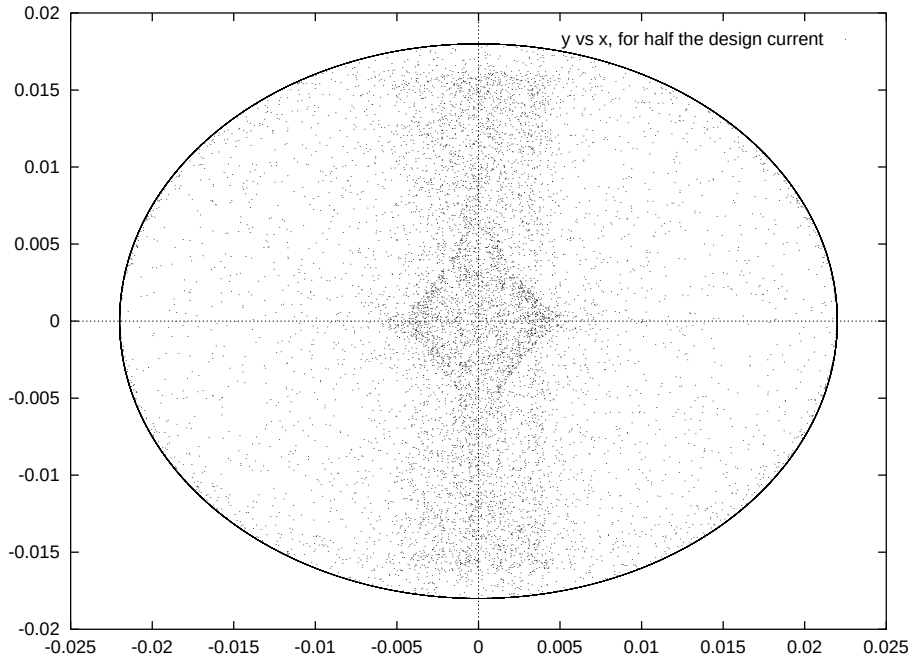

Figure 7: Transverse distribution of macroelectrons for half the design current per bunch, after 40 bunches for a maximum secondary emission yield δ_{max} of 1.7. Horizontal and vertical dimensions are given in units of m.

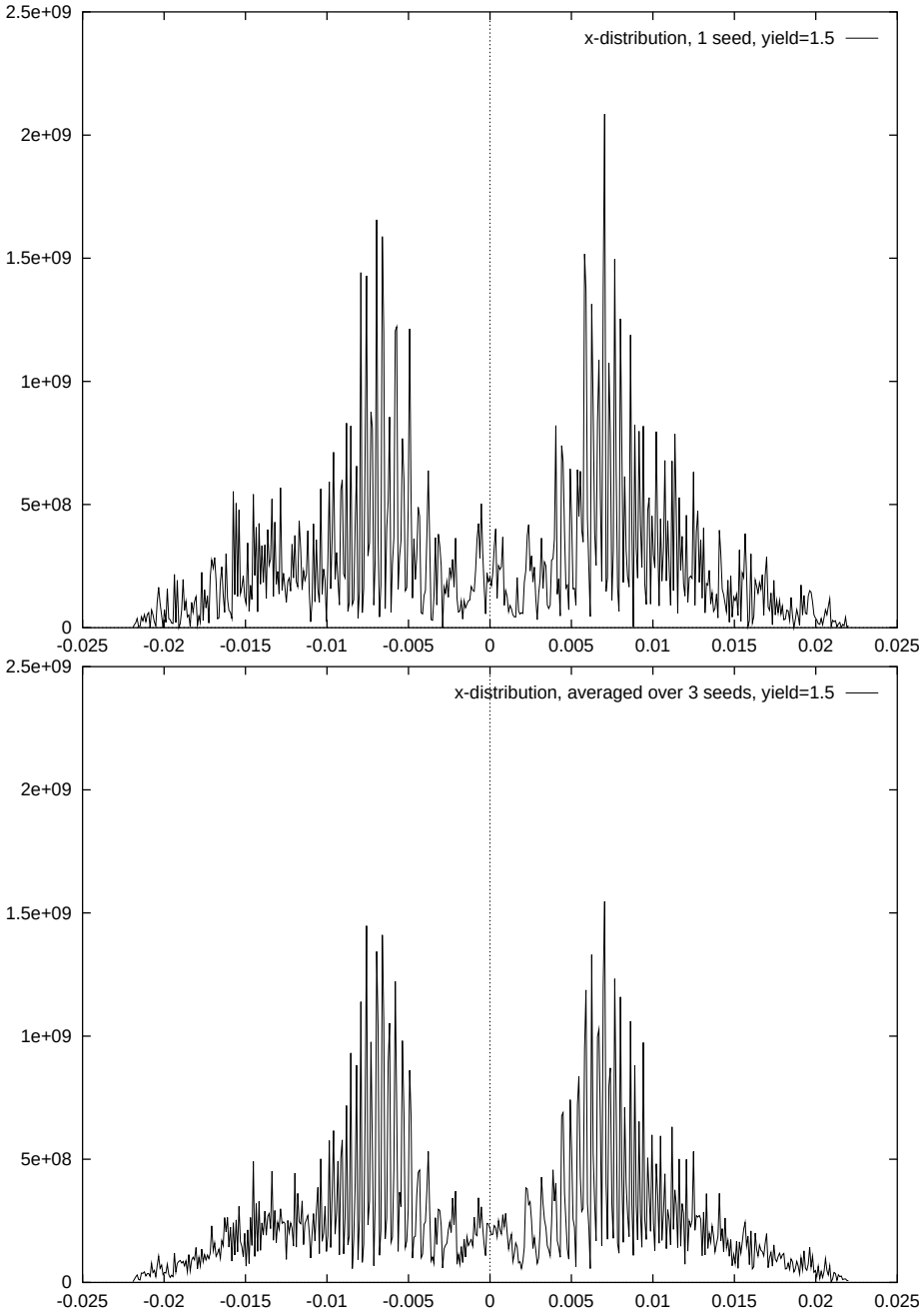

Figure 8: Projected horizontal electron charge density after 40 bunches, as obtained for one random seed (top) and averaged over three different seeds (bottom). The horizontal coordinate is given in units of meters; the vertical coordinate is the charge (in units of e) per bending magnet, per bin and per grid point. The total number of grid points is 500. The maximum yield is $\delta_{max} = 1.5$, and 1000 macroparticles per bunch (and per seed) were used.

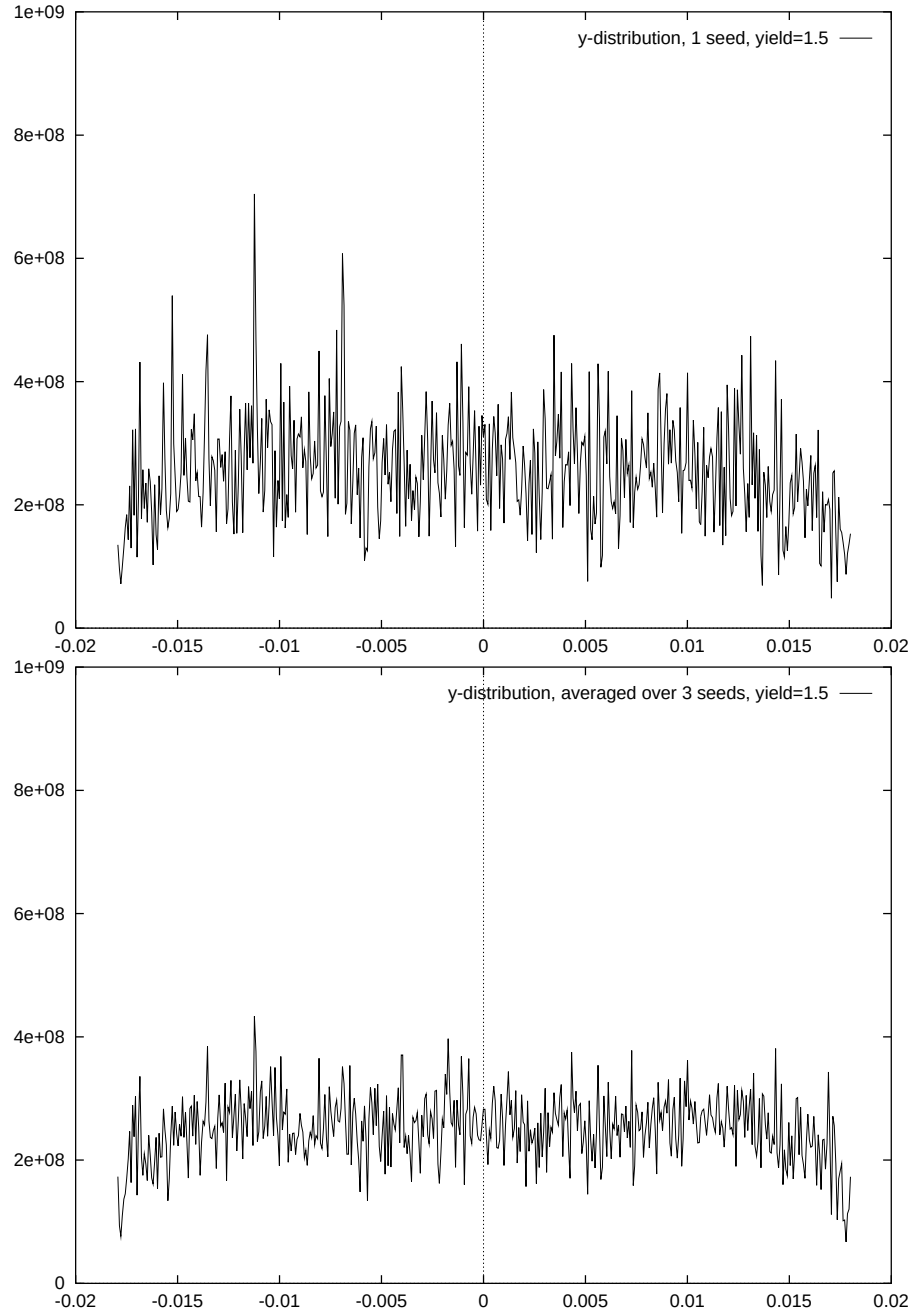

Figure 9: Projected vertical electron charge density after 40 bunches, as obtained for one random seed (top) and averaged over three different seeds (bottom). The horizontal coordinate is given in units of meters; the vertical coordinate is the charge (in units of e) per bending magnet, per bin and per grid point. The total number of grid points is 500. The maximum yield was chosen as $\delta_{max} = 1.5$, and 1000 macroparticles per bunch (and per seed) were used.

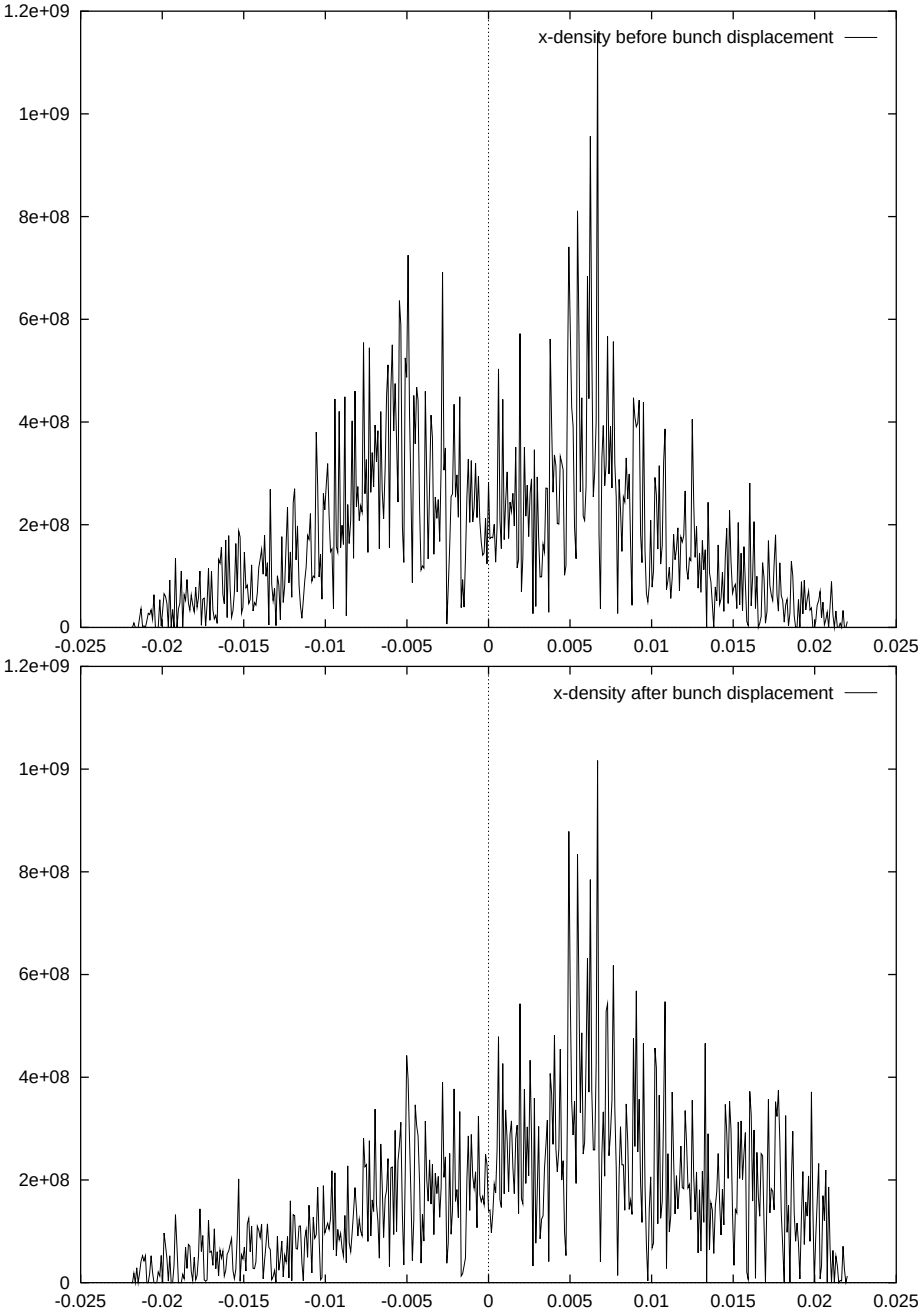

Figure 10: Projected horizontal electron charge density after about 40 bunches; top: before the 41st bunch is horizontally displaced by 1 cm; bottom: just prior to the arrival of the 42nd bunch. The horizontal axis is in units of meters; the vertical coordinate is the charge (in units of e) per bin and per grid point. The total number of grid points is 500. The maximum yield was chosen as $\delta_{max} = 1.7$, and 1000 macroparticles per bunch were used.

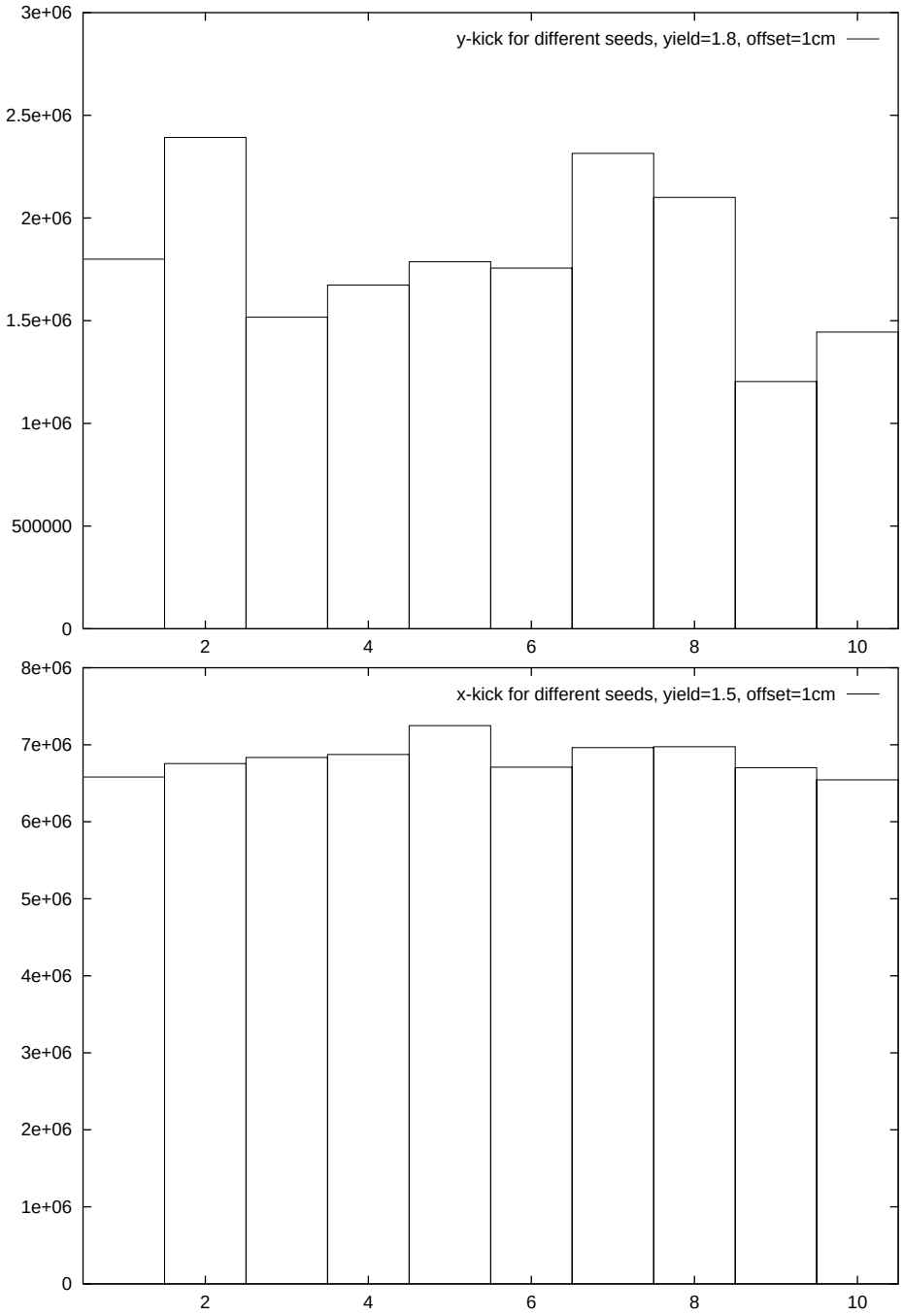

Figure 11: Vertical and horizontal wake function $W_1(L_{sep})$ in units of m^{-2} computed for 10 different random seeds. In these simulations, we assumed a maximum secondary-emission yield of $\delta_{max} = 1.8$ (top) and $\delta_{max} = 1.5$ (bottom). The vertical (horizontal) offset was Δy (Δx) = 1 cm, and 1000 (3000) macro-photoelectrons were launched per bunch. (Note that the average wake is $\sim 20\%$ larger than that listed in Table 2. This is due to both the smaller number of interbunch tracking steps (7 compared with 20 used for Table 2), and also the larger yield value $\delta_{max} = 1.8$ in the upper histogram.)

distribution also have some influence on the computed wakefield.

If the beam current is a factor 2 smaller than the design value (i.e., for $N_b \approx 5\times10^{10}$) the effective wakefield is reduced by about 40%. The wakefield does not decrease exactly in proportion to the beam current, because, for lower current, the high-density region of the electron cloud is closer to the beam-pipe center (Fig. 7).

Finally, reducing the number of photoelectrons emitted per photon by a factor of 5 results in a 40% smaller wakefield (in Table 2 this case is indicated by the comment '$\eta_{pe}^{eff} = 0.2$').

δ_{max}	mps./b.	section	Δy (Δx)	$W_{1,y}$ (10^5 m^{-2})	$W_{1,x}$ (10^6 m^{-2})	comment
1.5	1000	bend	1 cm	(9.7 ± 2.6)	(4.8 ± 0.2)	—
1.5	3000	bend	1 cm	(9.1 ± 1.0)	(5.1 ± 0.2)	—
1.5	1000	bend	5 mm	(12 ± 7)	(4.3 ± 0.8)	—
1.5	1000	bend	1 cm	not calc.	(2.9 ± 0.1)	$N_b = 5 \times 10^{10}$
1.5	1000	bend	1 cm	not calc.	(3.1 ± 0.1)	$\eta_{pe}^{eff} = 0.2$
1.1	1000	bend	1 cm	not calc.	(2.8 ± 0.3)	—
1.7	1000	bend	1 cm	not calc.	(6.1 ± 0.2)	—
1.5	1000	drift	1 cm	(3.5 ± 1.3)	(0.37 ± 0.24)	—

Table 2: Effective bunch-to-bunch dipole wake function after 40 bunches, extracted from the simulation, for various secondary emission yields, macroparticle numbers, transverse offsets, charges per bunch, and effective photoemission yields. The comment $\eta_{pe}^{eff} = 0.2$ refers to a reduction of the photoemission probability by a factor of 5, compared with the nominal case.

From Table 2, the integrated dipole wake functions $W_{1,x}^{LHC}(L_{sep})$ and $W_{1,y}^{LHC}(L_{sep})$ of Eq. (9) are about 4.1×10^6 m^{-2} and 0.8×10^6 m^{-6}, respectively. Inserting these values into Eq. (11), we estimate an instability rise time of 25 ms for the horizontal and of 130 ms for the vertical plane.

4 Conclusions

We have simulated the build-up of an electron cloud that is generated by photoemission and secondary emission in the LHC beam pipe. Based on the simulation results, the effect of the electron cloud on the beam stability was estimated. Our preliminary conclusion is that the electron cloud gives rise to a multi-bunch instability at top energy with an approximate rise time of the order of 25 ms in the horizontal and 130 ms in the vertical direction. The rise time is thus comparable to that of the resistive-wall instability at injection energy. The electron-cloud instability is driven primarily in the bending magnets, while the effective 'wakes' in the straight sections are 3–15 times smaller.

The LHC conditions do *not* seem to require a precise synchronism between electron motion and proton bunches, in order for the electron-cloud instability to become important. Since the simulation results show little change over a fairly wide range of parameters, they are probably not 'accidental'. That the electron-cloud instability has not been observed in other proton storage rings, such as HERA-p or the Tevatron, can be explained by the much lower critical energy (< 0.2 eV) in these machines: if the typical photon energy is much smaller than the work function of the beam-pipe material, the probability of photoemission is reduced by many orders of magnitude.

To safely damp the electron-cloud instability, a bunch-by-bunch feedback system with a response time of about 10 ms will be necessary. Even if it is damped by such

a feedback system, the instability may still lead to an incoherent emittance growth. Also higher-order instability modes (e.g., quadrupole, sextupole mode...) could occur [25]. These modes may be excited by the beam-beam interaction [25] and are not easily damped by a feedback. As an alternative cure, the instability growth rate may be decreased by introducing additional gaps in the bunch train. In a gap of 2–3 bunch places almost all electrons will be lost. Our simulations suggest that such gaps must occur very frequently, i.e., about every 5–10 bunches.

All the results presented are preliminary. In the future, the simulations can be improved and extended in various regards, for instance, by

1. solving the Poisson equation with a 2-dim. FFT or by using a 2-dim. particle-in-cell code to more accurately represent the electron space-charge field,
2. including the effect of the magnetic field of the beam on the electron motion,
3. a fully relativistic treatment of the electron motion in all three directions,
4. using the real beam-screen dimensions instead of an elliptical approximation,
5. calculating the effective quadrupole wakefield, and
6. a careful revision of all the underlying assumptions.

The secondary emission yield of a copper vacuum chamber can be reduced by coating with an appropriate material such as TiN or TiZr [26]. Measurements of secondary emission and photoemission on vacuum-chamber prototypes would be a useful input for future studies. In particular, the sensitivity of the secondary-emission yield to a strong magnetic field, its dependence on the incident angle and the effect of physisorbed hydrogen molecules at the beam-screen surface should be investigated. One may also hope to reduce the photoemission yield by special surface treatments.

Finally, it should be mentioned that, in addition to causing a transverse beam instability, the large number of electrons bouncing in the beam pipe will raise the average vacuum pressure and the heat load on the cryogenic system. These aspects will require more detailed studies.

Acknowledgements

I would like to thank Francesco Ruggiero for guidance, help, discussions during the course of this work and a careful reading of the manuscript. Miguel Furman, Sam Heifets, Tor Raubenheimer, Oswald Gröbner, Cristoforo Benvenuti, Glen Lambertson, John Seeman, Mike Zisman, and Wolfgang Stoeffl deserve my warm thanks for many useful informations and various stimulating discussions. The work reported here has been strongly inspired by similar simulation studies which Miguel Furman has recently performed for PEP-II, and by Sam Heifets' analytical calculations.

I also want to thank the AP group of the CERN SL division, in particular Francesco Ruggiero, Jacques Gareyte and Jean-Pierre Koutchouk, for the invitation to CERN, hospitality and support. Lastly, I thank Michael Böge and Hans Grote for help with the CERN computer system.

References

[1] K. Ohmi, Phys. Rev. Lett., Vol. 75, No. 8 (1995).
[2] O. Gröbner, 10th Int. Conference on High Energy Accelerators, Protvino (1977).
[3] The Large Hadron Collider, Conceptual Design, CERN/AC/95-05 (1995); note that the dimensions of the beam screen have been slightly increased to the values quoted, since this report was written.
[4] M. Izawa et al., Phys. Rev. Lett., Vol. 74 No. 8 (1995).

[5] S. Kurokawa, private communication (1997).
[6] M. Furman and G. Lambertson, talk for PEP-II Machine Advisory Committee and updates, January 1997 (1997).
[7] S.A. Heifets, "Transverse Instability Driven by Trapped Electrons", SLAC/AP-95-101 (1995).
[8] W. Stoeffl, private communication (1994).
[9] O. Gröbner, "Technological problems related to the cold vacuum system of the LHC", Vacuum, vol. 47, pp. 591–595 (1996).
[10] H.G. Hereward, CERN 71-15 (1971).
[11] E. Keil and B. Zotter, CERN-ISR-TH/71-58 (1971).
[12] M. Sands, "The Physics of Electron Storage Rings", SLAC-121 (1970).
[13] J. Kouptsidis and G.A. Mathewson, DESY 76/49 (1976).
[14] World-wide web page 'http://www-crxo.lbl.gov/optical_constants/' published by the LBNL X-ray laboratory.
[15] M. Furman, private communication (1996).
[16] M. Zisman, private communication (1996).
[17] S. Heifets, private communication (1997).
[18] H. Bruining, "Physics and Applications of Secondary Electron Emission", Pergamon Press (1954).
[19] H. Seiler, "Secondary electron emission in the scanning electron microscope", J. Appl. Phys. 54 (11) (1983).
[20] M. Furman, private communication (1996).
[21] The importance of this effect, in particular for the PEP-II chamber, was mentioned by T. Raubenheimer (1997).
[22] F. Ruggiero, private suggestion (1997).
[23] T. Raubenheimer, private communication (1997).
[24] A. Chao, "Physics of Collective Beam Instabilities in High Energy Accelerators", Wiley, p. 208 (1995).
[25] J. Gareyte, private communication (1997).
[26] C. Benvenuti, private communication (1997).